Supporting Information

Electronic Functionality Encoded Laser-Induced Graphene for Paper Electronics

Hyunjin Park[†,⊥], *Minsu Kim*[†,⊥], *Byoung Gak Kim*[†,‡,*], *and Yun Ho Kim*[†,‡,*]

[†]Advanced Materials Division, Korea Research Institute of Chemical Technology (KRICT), Daejeon 34114, Republic of Korea.

[‡]KRICT School, University of Science and Technology (UST), Daejeon 34113, Republic of Korea.

* Corresponding authors: bgkim@krict.re.kr, yunho@krict.re.kr

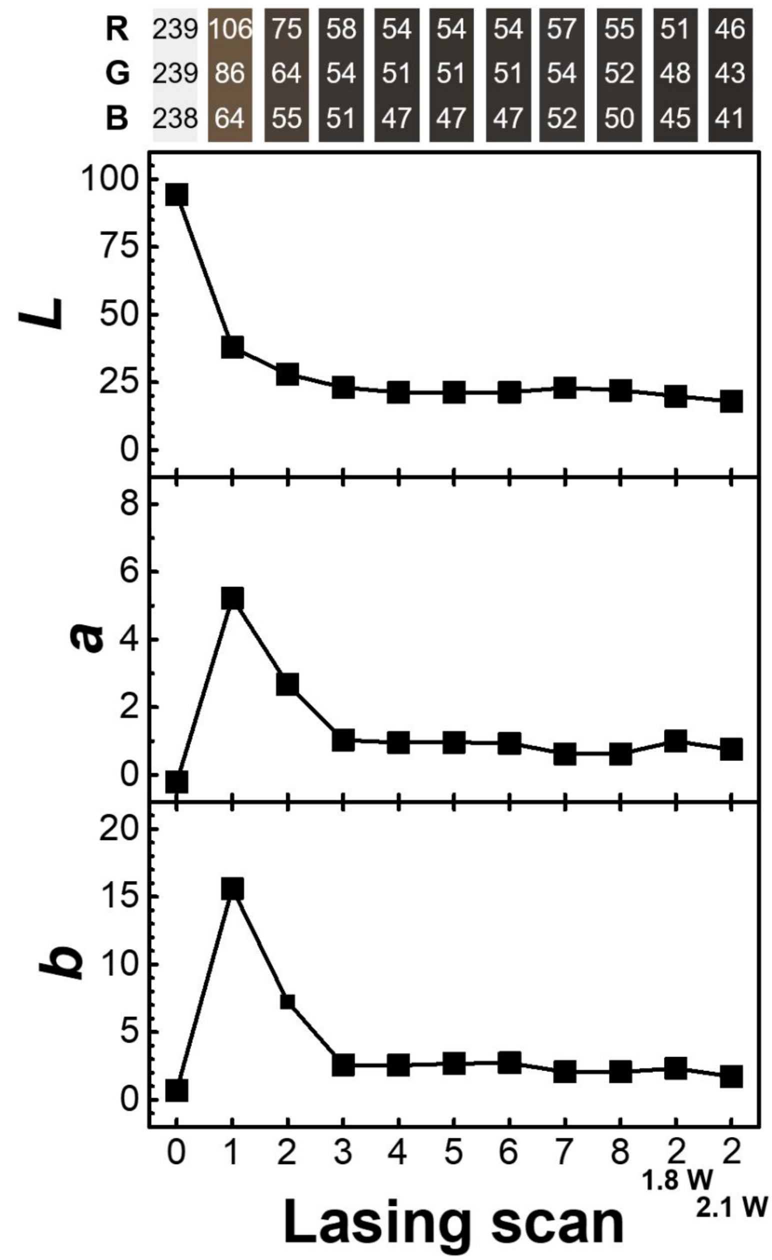

Figure S1. Reflectance spectra of paper-derived LIG with various lasing conditions recorded using spectrophotometer in *L*, *a*, and *b* values. The topmost panel represents the assigned color of the red-green-blue (RGB) system converted from the lightnesschromaticity coordinate (LAB) system. In the LAB color system, +a, −a, +b, and –b represent red, green, yellow, and blue axis, respectively.

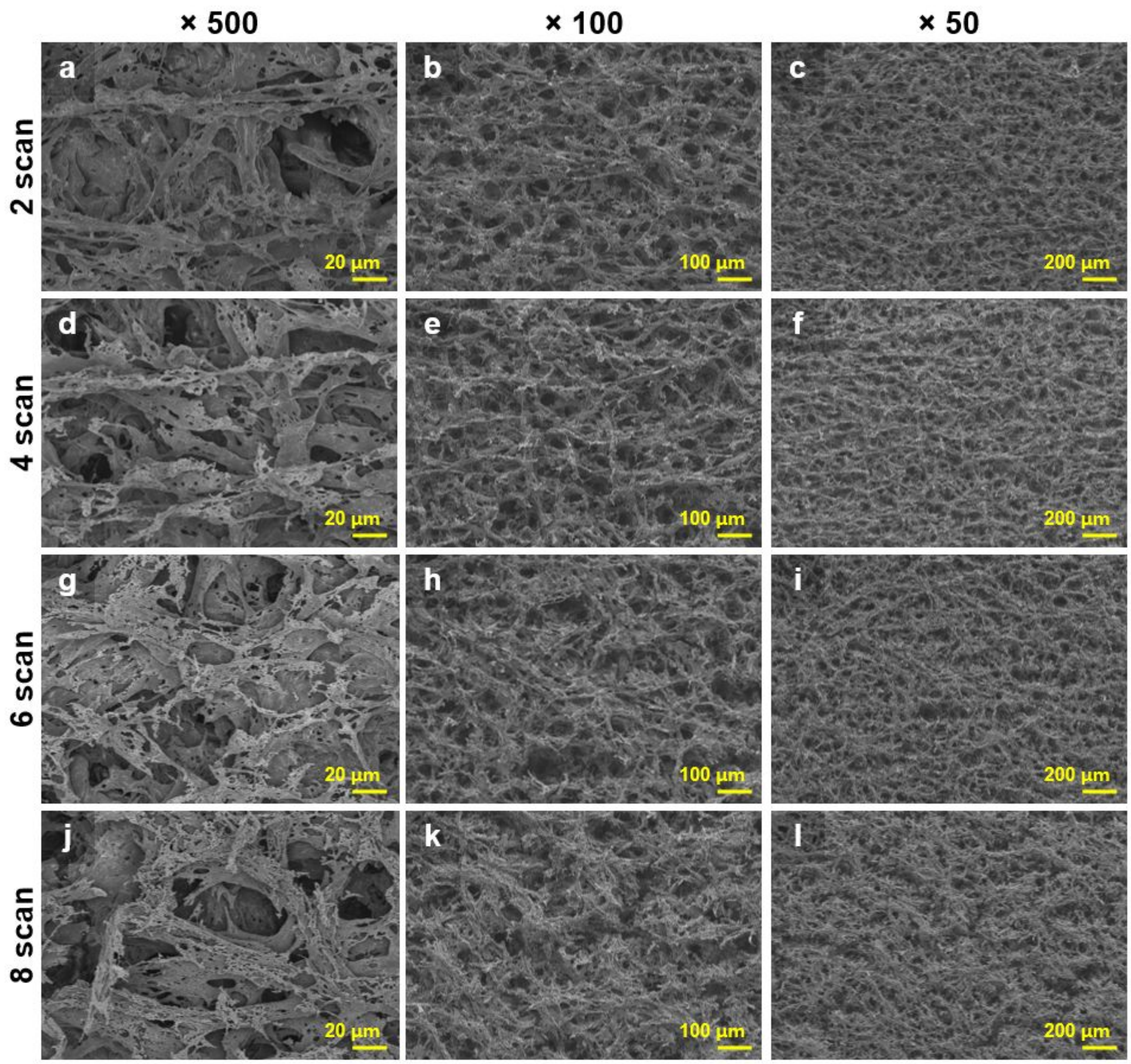

Figure S2. (a-l) Top view SEM images of paper-derived LIG with (a-c) 2, (d-f) 4, (g-i) 6, and (j-l) 8 lasing scans at 1.5 W. The SEM images are recorded at (a,d,g,j) 500, (b,e,h,k) 100, and (c,f,i,l) 50 magnifications.

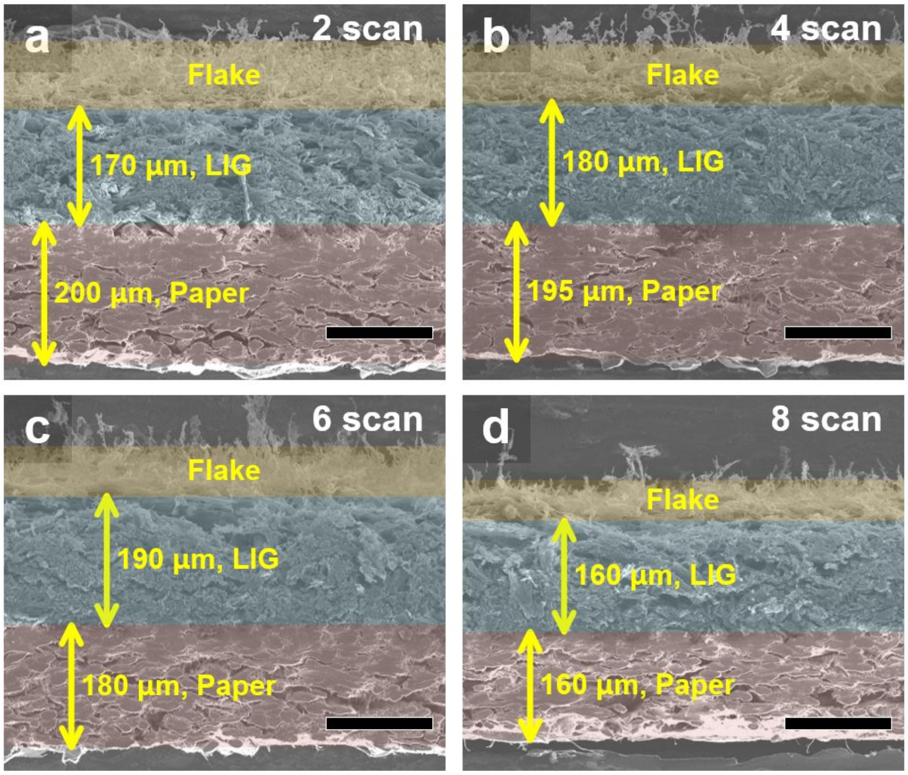

Figure S3. (a-d) Cross-sectional SEM images of paper-derived LIG with (a) 2, (b) 4, (c) 6, and (d) 8 lasing scans at 1.5 W. The scale bar represents 150 µm.

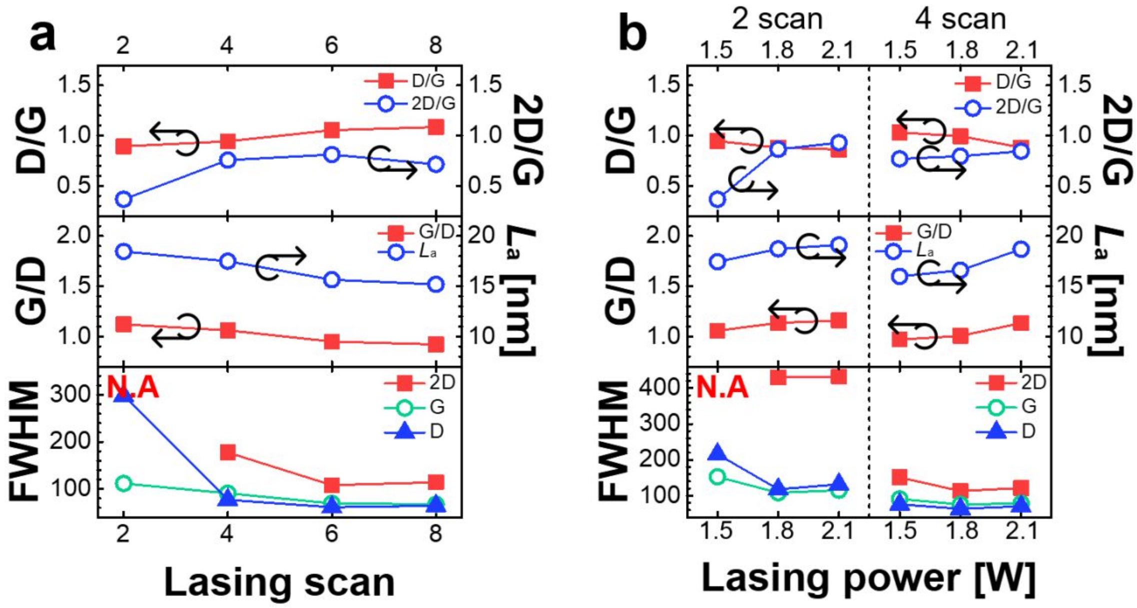

Figure S4. (a,b) Statistical analysis of Raman spectra for D/G and 2D/G peak ratios (top), G/D peak ratio and L_a (middle), and FWHM of D, G, and 2D bands (bottom) as function of (a) number of lasing scans and (b) lasing power.

To quantitatively compare the graphitization degree of paper-derived LIG, the Raman peak ratios of D and G (D/G = I_D/I_G^{-1}) and 2D and G (2D/G = I_{2D}/I_G^{-1}) were estimated to determine the degree of defects and the number of graphene layers, respectively.[1–4] For the lasing power of 1.5 W, the D/G and 2D/G ratios of LIG gradually increased from 0.94 to 1.09 and 0.37 to 0.81, respectively, with multiple lasing scans (top panel of Figure S4a).

However, the LIG with 8 lasing scans showed slightly lower 2D/G ratio of 0.71 due to the excessive energy absorption leading to the deteriorated LIG structure.[5] The estimated D/G and 2D/G ratios imply that the LIG contains more defects and number of graphene layers in the structure with multiple lasing scans. In contrast, with higher lasing power, the D/G ratio decreased from 0.94 to 0.86 and 1.03 to 0.88 for 2 and 4 lasing scans, respectively, whereas the 2D/G ratio increased from 0.37 to 0.93 and 0.76 to 0.84 for 2 and 4 lasing scans, respectively (top panel of Figure S4b). The results indicate that a higher lasing power leads to a higher graphitization degree of LIG while more graphene layers are obtained.

Raman spectroscopy is a powerful analysis technique to obtain the average grain size of graphene along the *a*-axis (L_a) by estimating the G and D peak ratio (G/D= I_G/I_D^{-1}) with the following equation:[6]

$$L_a = (2.4 \times 10^{-10}) \times \lambda_l^4 \times (\frac{I_G}{I_D}), \qquad (1)$$

where λ_l is the wavelength of the Raman spectroscopy (= 512 nm). The estimated L_a decreased from 17.43 to 15.18 nm with multiple lasing scans (middle panel of Figure

S4a). On the other hand, a higher lasing power leads to a larger L_a up to 19.12 and 18.69 nm for 2 and 4 lasing scans, respectively, and is attributed to the partial oxidation of LIG in the air (middle panel of Figure S4b).[2] The full width at half maximum (FWHM) of D, G, and 2D bands remarkably decreased with multiple lasing scans and higher lasing power, indicating that LIG experienced a good graphitization reaction (bottom panel of Figure S4). All estimated parameters are summarized in Table S1. When the parameters were compared, the graphitization degree of paper-derived LIG was comparable to LIG produced on polymer substrates (Table S2).

Table S1. Statistical analysis of Raman spectra of LIG with various lasing conditions.

Lasing scan	Lasing power [W]	D/G	2D/G	L_a [nm]	R_{sh} [Ω·sq^{-1}]	FWHM [cm^{-1}]		
						2D	G	D
2	1.5	0.94	0.37	17.43	9140	N.A	152.60	215.79
4		1.03	0.76	15.99	178	151.07	90.80	75.94
6		1.05	0.81	15.65	183	108.03	69.38	61.20
8		1.09	0.71	15.18	168	114.14	67.37	64.38
2	1.8	0.88	0.86	18.73	1080	429.78	108.12	117.97
4		0.99	0.79	16.59	177	112.95	75.42	63.25
2	2.1	0.86	0.93	19.12	866	432.09	115.39	131.61
4		0.88	0.84	18.69	83	121.55	78.51	70.62

Table S2. Comparison of Raman spectra with previously reported works.

Ref.	Author	Substrate	D/G	2D/G	L_a [nm]	R_{sh} [Ω·sq^{-1}]	2D	G	D
7	Matteo Parmeggiani	PDMS, PI	0.72	0.61*	23.27	80	–	–	–
8	Yieu Chyan	PEI	0.2	0.65	83.76*	15	–	35	–
		Coconut	0.52*	0.75*	32.22*	–	–	–	–
		Potato	0.66*	0.7*	25.38*	–	–	–	–
		Paper	1.05*	0.47*	15.95*	–	–	–	–
2	Jian Lin	PI	0.44	0.88*	40	15	60	–	–
9	Michael G. Stanford	PI	0.79*	0.79*	–	40	–	–	–
		Cork	0.54*	0.58*		115			
10	Duy Xuan Luong	PI	–	–	–	20	–	–	–
11	Yieu Chyan	Paper	1	0.52*	16*	40	–	–	–
12	Yilun Li	PI	0.6-0.8	0.6-0.7	20.94-27.92	–	–	–	–
13	Fangcheng Wang	GO/Urea	0.66	1.46	58.38	–	61.44	37.85	78.91
5	Chenguang Zhu	PEEK	0.75	–	51.4	–	–	–	–
14	Macro R. Bobinger	PI	–	–	–	250	–	–	–
	This work	Paper User	1.05	0.81	15.65	183	108.03	69.38	61.20
		Paper Best	0.88	0.84	18.69	83	121.5	78.51	70.62

5

PDMS: polydimethylsiloxane; PI: polyimide; PEI: poly(ether imide); GO: graphene oxide; PEEK: polyether ether ketone

*This notation indicates that the value is not provided in the paper, but roughly estimated from the figure.

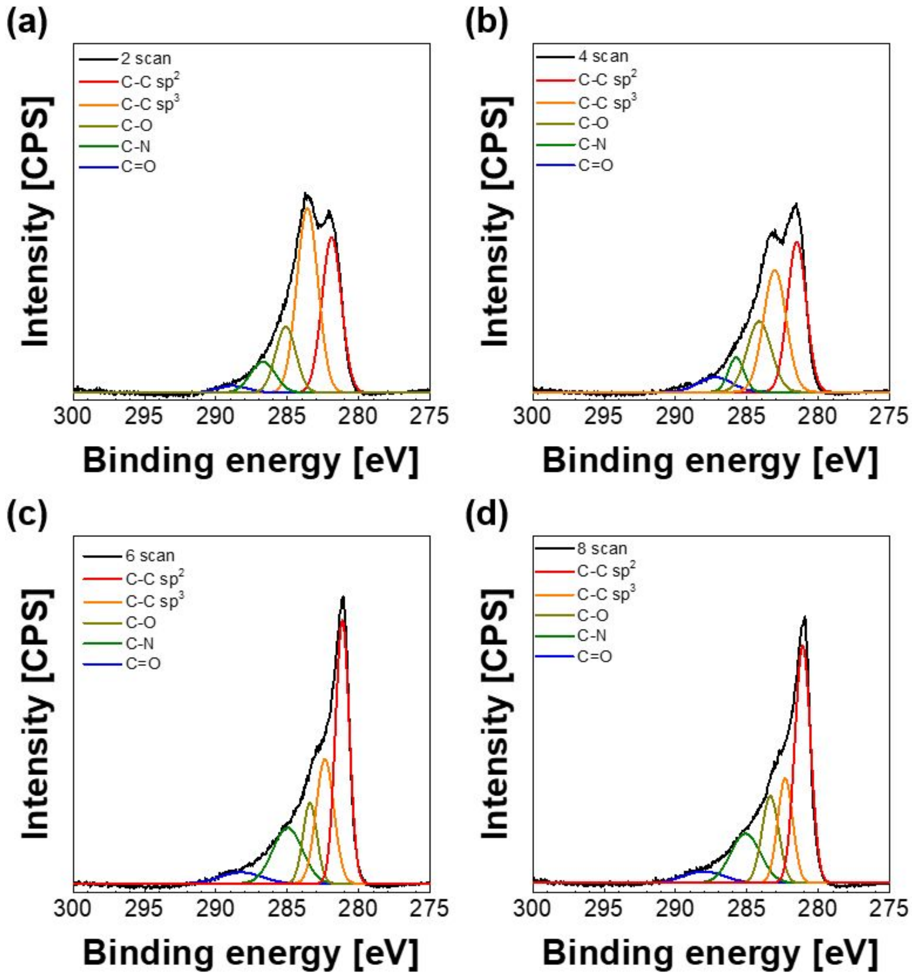

Figure S5. Deconvolution of XPS C1 s for LIG with (a) 2, (b) 4, (c) 6, and (d) 8 lasing scans.

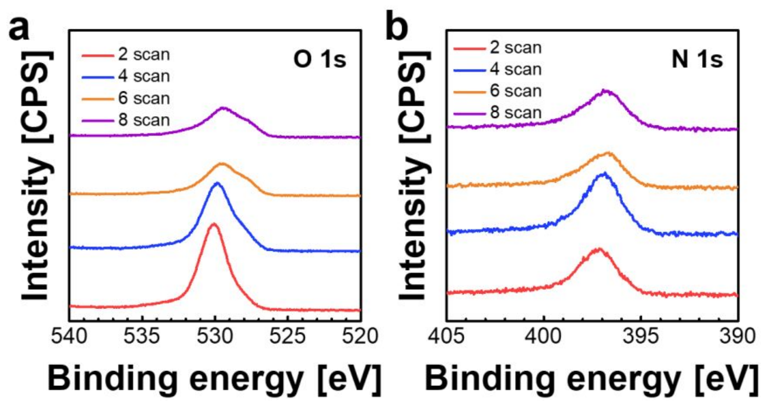

Figure S6. (a,b) XPS spectra of (a) O 1s and (b) N 1s for LIG with various number of lasing scans.

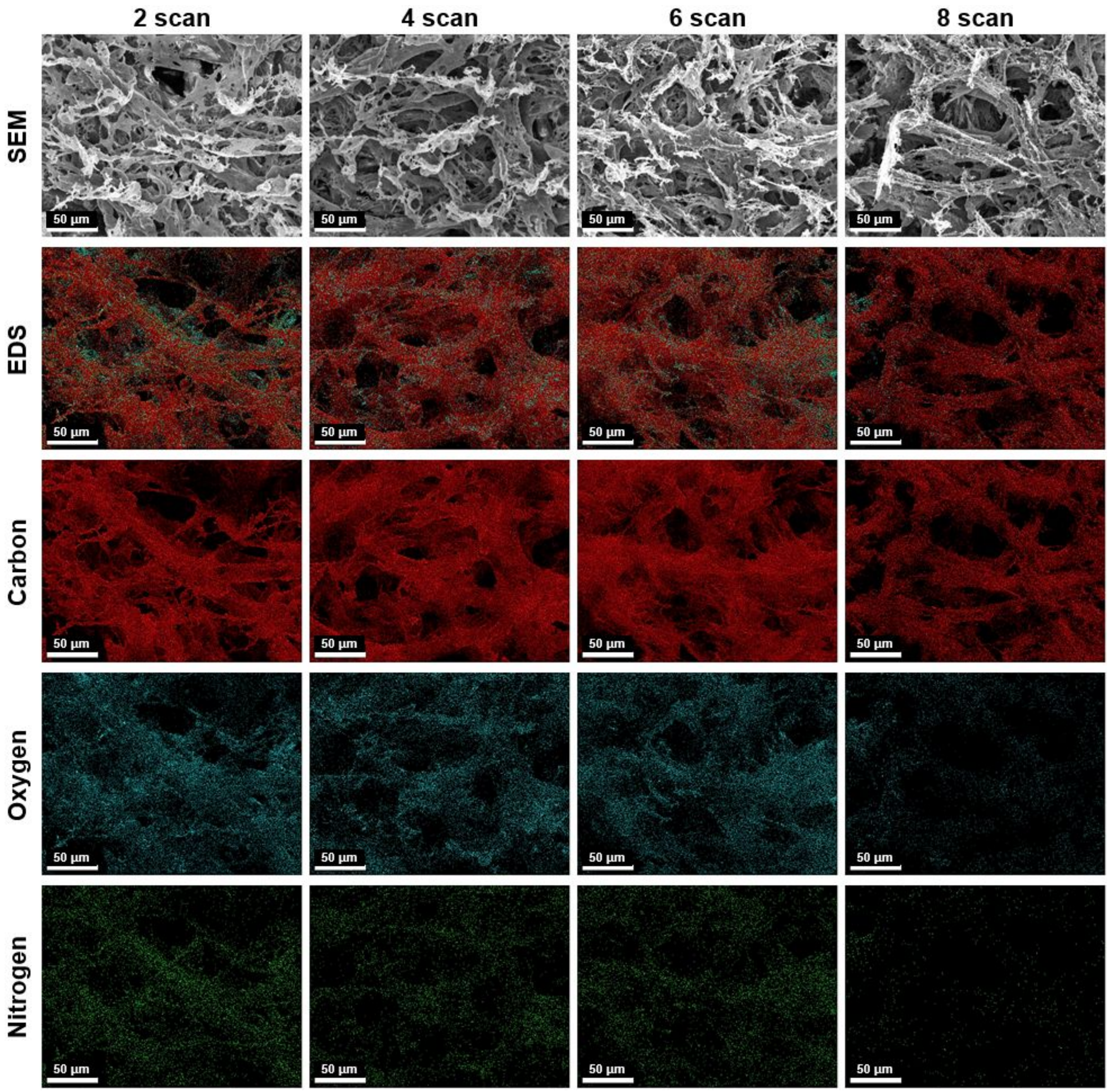

Figure S7. SEM/EDS images of C, O and N with 2, 4, 6, and 8 lasing scans. The scale bar represents 50 μm.

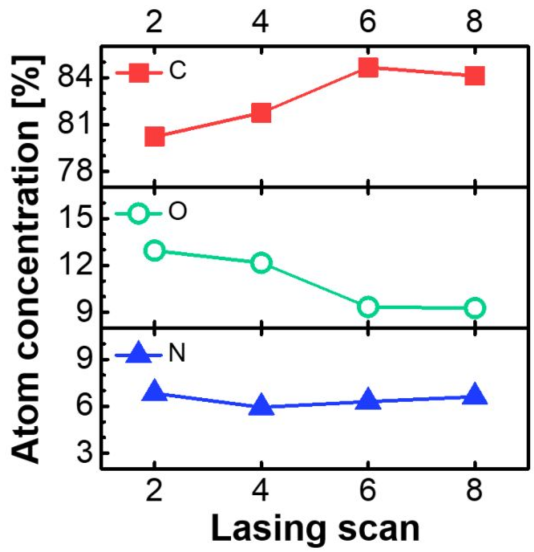

Figure S8. SEM/EDS analysis to identify the atom concentration of C (top), O (middle), and N (bottom).

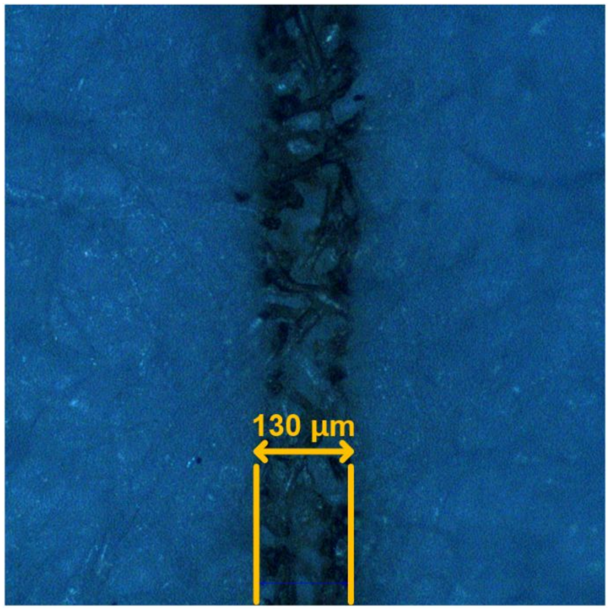

Figure S9. Minimum feature size of LIG line prepared at 1.5 W with 8 lasing scans.

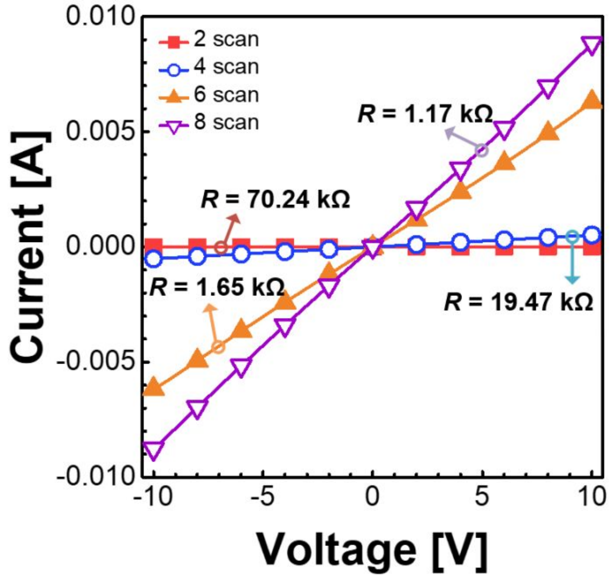

Figure S10. Linearity of R_{LIG} having 5 mm and 500 μm of length and width, respectively, as function of voltage bias.

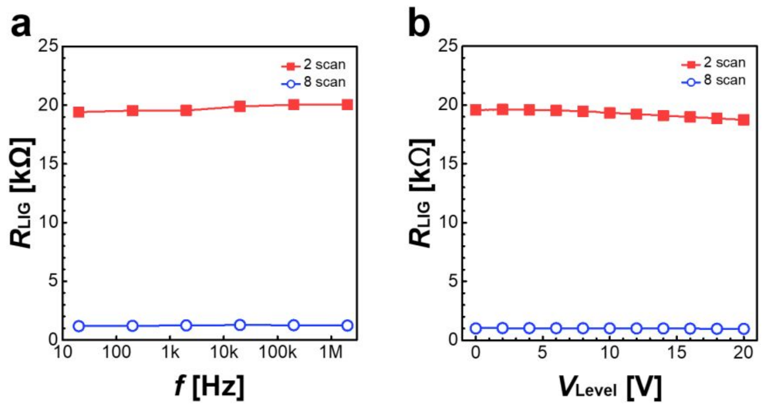

Figure S11. (a,b) R_{LIG} with 2 and 8 lasing scans as function of (a) f and (b) V_{Level}.

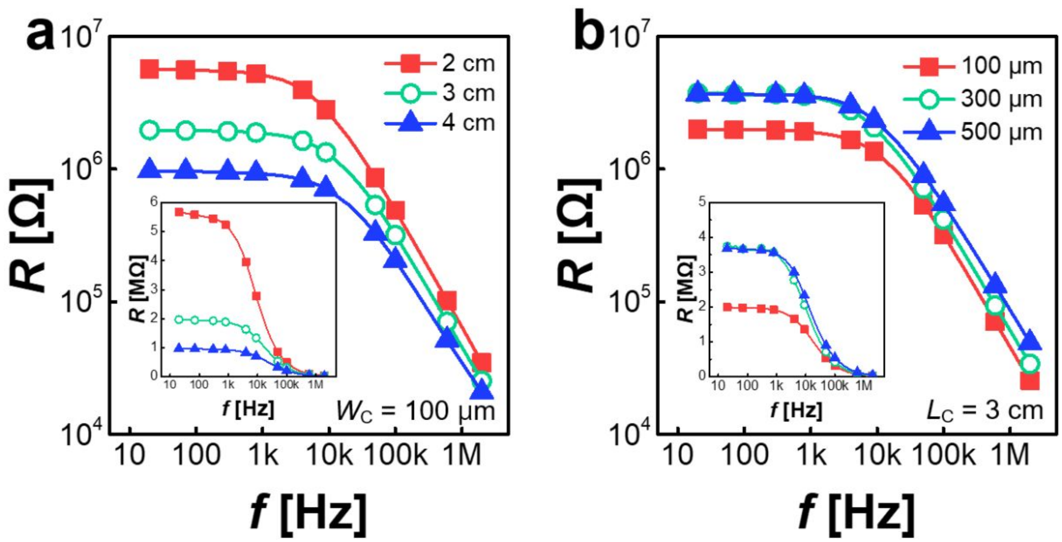

Figure S12. (a,b) Resistance of LIG-capacitor in logarithm scale with various (a) L_C and (b) W_C as function of *f*. The insets show the resistance of LIG-capacitor in linear scale.

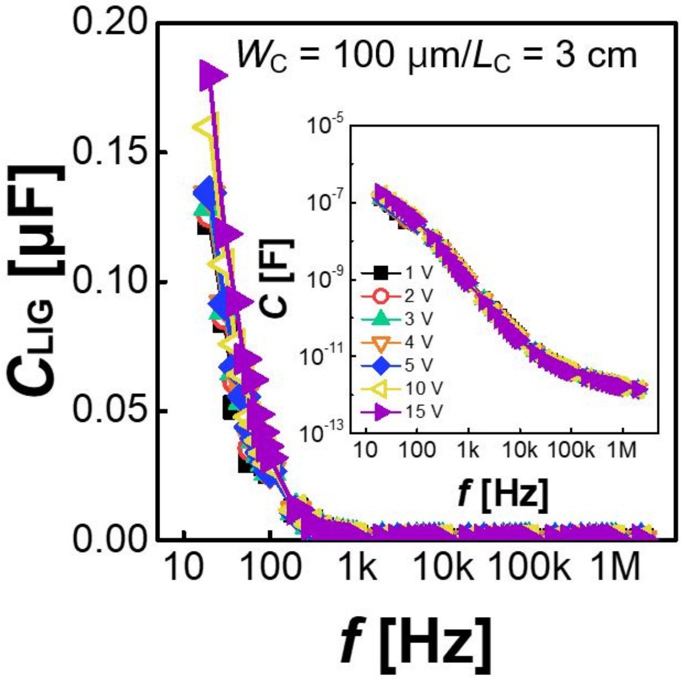

Figure S13. C_{LIG} in linear scale with various voltage level as function of frequency. The inset represents the C_{LIG} in logarithm scale.

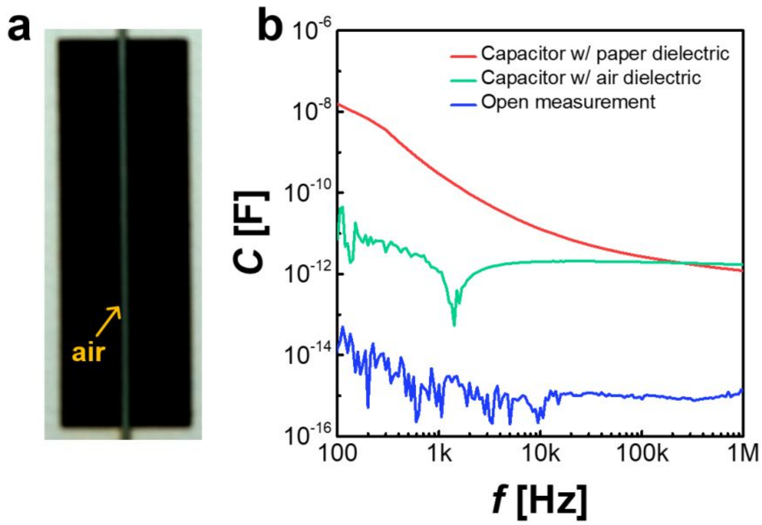

Figure S14. (a) Photograph image of LIG-capacitor with air dielectric. (b) Capacitance of LIG-capacitor with paper and air dielectrics.

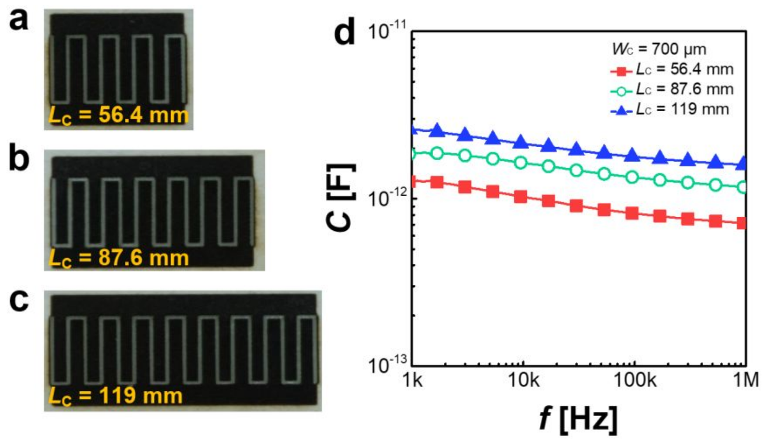

Figure S15. (a-c) Photograph images of LIG-capacitors with air dielectric having L_C of (a) 56.4 mm, (b) 87.6 mm, (c) 119 mm. (d) Capacitance of LIG-capacitors as function of frequency.

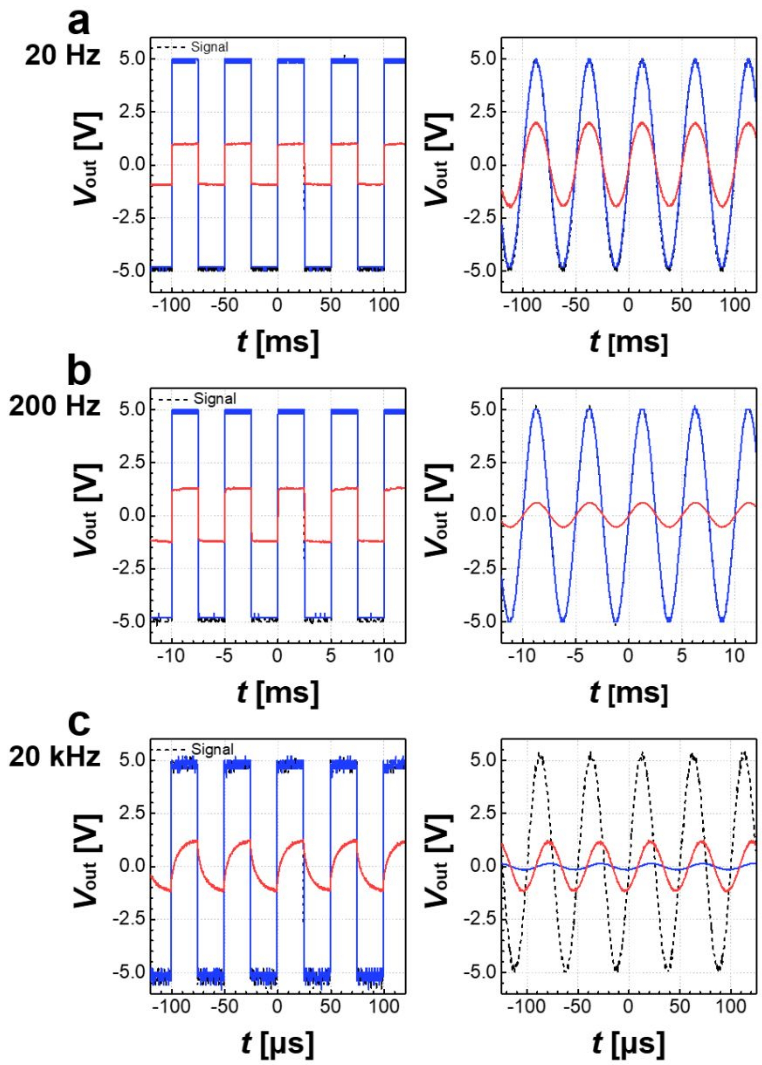

Figure S16. (a-c) Output signals of RC circuits with input signals of square (left column) and sinusoidal (right column) waveforms at (a) 20 Hz, (b) 200 Hz, and (c) 20 kHz. The black line represents the input signal and the blue and red lines represent the output signals of RC circuit A and B, respectively.

REFERENCES

(1) Allen, M. J.; Tung, V. C.; Kaner, R. B. Honeycomb Carbon: A Review of Graphene. *Chem. Rev.* **2010**, *110* (1), 132–145. https://doi.org/10.1021/cr900070d.

(2) Lin, J.; Peng, Z.; Liu, Y.; Ruiz-Zepeda, F.; Ye, R.; Samuel, E. L. G.; Yacaman, M. J.; Yakobson, B. I.; Tour, J. M. Laser-Induced Porous Graphene Films from Commercial Polymers. *Nat. Commun.* **2014**, *5* (1), 5714. https://doi.org/10.1038/ncomms6714.

(3) Ferrari, A. C.; Meyer, J. C.; Scardaci, V.; Casiraghi, C.; Lazzeri, M.; Mauri, F.; Piscanec, S.; Jiang, D.; Novoselov, K. S.; Roth, S.; Geim, A. K. Raman Spectrum of Graphene and Graphene Layers. *Phys. Rev. Lett.* **2006**, *97* (18), 187401. https://doi.org/10.1103/PhysRevLett.97.187401.

(4) Liu, X.; Chao, D.; Su, D.; Liu, S.; Chen, L.; Chi, C.; Lin, J.; Shen, Z. X.; Zhao, J.; Mai, L.; Li, Y. Graphene Nanowires Anchored to 3D Graphene Foam via Self-

Assembly for High Performance Li and Na Ion Storage. *Nano Energy* **2017**, *37* (February), 108–117. https://doi.org/10.1016/j.nanoen.2017.04.051.

(5) Zhu, C.; Zhao, D.; Wang, K.; Dong, X.; Duan, W.; Wang, F.; Gao, M.; Zhang, G. Direct Laser Writing of Graphene Films from a Polyether Ether Ketone Precursor. *J. Mater. Sci.* **2019**, *54* (5), 4192–4201. https://doi.org/10.1007/s10853-018-3123-5.

(6) Cançado, L. G.; Takai, K.; Enoki, T.; Endo, M.; Kim, Y. A.; Mizusaki, H.; Jorio, A.; Coelho, L. N.; Magalhães-Paniago, R.; Pimenta, M. A. General Equation for the Determination of the Crystallite Size La of Nanographite by Raman Spectroscopy. *Appl. Phys. Lett.* **2006**, *88* (16), 163106. https://doi.org/10.1063/1.2196057.

(7) Parmeggiani, M.; Zaccagnini, P.; Stassi, S.; Fontana, M.; Bianco, S.; Nicosia, C.; Pirri, C. F.; Lamberti, A. PDMS/Polyimide Composite as an Elastomeric Substrate for Multifunctional Laser-Induced Graphene Electrodes. *ACS Appl. Mater. Interfaces* **2019**, *11* (36), 33221–33230. https://doi.org/10.1021/acsami.9b10408.

(8) Chyan, Y.; Ye, R.; Li, Y.; Singh, S. P.; Arnusch, C. J.; Tour, J. M. Laser-Induced Graphene by Multiple Lasing: Toward Electronics on Cloth, Paper, and Food. *ACS Nano* **2018**, *12* (3), 2176–2183. https://doi.org/10.1021/acsnano.7b08539.

(9) Stanford, M. G.; Li, J. T.; Chyan, Y.; Wang, Z.; Wang, W.; Tour, J. M. Laser-Induced Graphene Triboelectric Nanogenerators. *ACS Nano* **2019**, *13* (6), 7166–7174. https://doi.org/10.1021/acsnano.9b02596.

(10) Luong, D. X.; Yang, K.; Yoon, J.; Singh, S. P.; Wang, T.; Arnusch, C. J.; Tour, J. M. Laser-Induced Graphene Composites as Multifunctional Surfaces. *ACS Nano* **2019**, *13*, acsnano.8b09626. https://doi.org/10.1021/acsnano.8b09626.

(11) Chyan, Y.; Cohen, J.; Wang, W.; Zhang, C.; Tour, J. M. Graphene Art. *ACS Appl. Nano Mater.* **2019**, *2* (5), 3007–3011. https://doi.org/10.1021/acsanm.9b00391.

(12) Li, Y.; Luong, D. X.; Zhang, J.; Tarkunde, Y. R.; Kittrell, C.; Sargunaraj, F.; Ji, Y.; Arnusch, C. J.; Tour, J. M. Laser-Induced Graphene in Controlled Atmospheres: From Superhydrophilic to Superhydrophobic Surfaces. *Adv. Mater.* **2017**, *29* (27), 1700496. https://doi.org/10.1002/adma.201700496.

(13) Wang, F.; Dong, X.; Wang, K.; Duan, W.; Gao, M.; Zhai, Z.; Zhu, C.; Wang, W. Laser-Induced Nitrogen-Doped Hierarchically Porous Graphene for Advanced Electrochemical Energy Storage. *Carbon N. Y.* **2019**, *150*, 396–407. https://doi.org/10.1016/j.carbon.2019.05.037.

(14) Bobinger, M. R.; Romero, F. J.; Salinas-Castillo, A.; Becherer, M.; Lugli, P.; Morales, D. P.; Rodríguez, N.; Rivadeneyra, A. Flexible and Robust Laser-Induced Graphene Heaters Photothermally Scribed on Bare Polyimide Substrates. *Carbon N. Y.* **2019**, *144*, 116–126. https://doi.org/10.1016/j.carbon.2018.12.010.